Sensors & Actuators: B. Chemical 281 (2019) 960–970

Contents lists available at ScienceDirect

Sensors and Actuators B: Chemical

journal homepage: www.elsevier.com/locate/snb

Simple and ultrafast resonance frequency and dissipation shift measurements using a fixed frequency drive

Arnab Guha[a], Niklas Sandström[b], Victor P. Ostanin[c], Wouter van der Wijngaart[b], David Klenerman[c], Sourav K. Ghosh[a,*]

[a] Centre for Biological Engineering, Loughborough University, Loughborough, UK
[b] Micro and Nanosystems, KTH Royal Institute of Technology, Stockholm, Sweden
[c] Department of Chemistry, University of Cambridge, Cambridge, UK

ARTICLE INFO

Keywords:
Acoustic sensor
Quartz crystal microbalance
Resonance frequency shift
Dissipation shift
Realtime monitoring
Time resolution of biomolecular process measurement

ABSTRACT

A new method for determination of resonance frequency and dissipation of a mechanical oscillator is presented. Analytical expressions derived using the Butterworth-Van Dyke equivalent electrical circuit allow the determination of resonance frequency and dissipation directly from each impedance datapoint acquired at a fixed amplitude and frequency of drive, with no need for numerical fitting or measurement dead time unlike the conventional impedance or ring-down analysis methods. This enables an ultrahigh time resolution and superior noise performance with relatively simple instrumentation. Quantitative validations were carried out successfully against the impedance analysis method for inertial and viscous loading experiments on a 14.3 MHz quartz crystal resonator (QCR). Resonance frequency shifts associated with the transient processes of quick needle touches on a thiol self-assembled-monolayer functionalised QCR in liquid were measured with a time resolution of 112 μs, which is nearly two orders of magnitude better than the fastest reported quartz crystal microbalance. This simple and fast fixed frequency drive (FFD) based method for determination of resonance frequency and dissipation is potentially more easily multiplexable and implementable on a single silicon chip delivering economies of scale.

1. Introduction

Resonance frequency and dissipation measurements of mechanical oscillators, such as quartz crystal resonators (QCR) and cantilevers, are widely used in electrochemistry [1–4], surface science [5–7] and biosensors [8–11] to quantify processes on the surface. Traditionally, oscillators with frequency counters and automatic gain control [12–16], impedance analysis of a frequency sweep [17–23] and voltage ring-down analysis [24–27] have been the most commonly used methods for measuring the resonance frequency and dissipation factor (inverse of Quality factor) of an oscillator. State-of-the-art instruments now report these measurements at multiple resonance modes or overtones [28–30]. However, the time resolution, i.e. the time for measurement of one resonance frequency or dissipation datapoint, is limited in most practical cases, with a trade-off between the speed of data acquisition and noise.

In impedance analysis method, an oscillator is driven by sweeping the frequency spanning around its nominal resonance frequency and the admittance spectrum is fitted with an equivalent electrical circuit to estimate the resonance frequency and dissipation. The frequency sweep needs to have a minimal number of steps in order to achieve an acceptable quality of the nonlinear fitting, with the time per step inversely proportional to the resonance bandwidth to avoid artefacts from transient processes. Moreover, there is a dead time between successive data acquisitions to reduce transient interference that affects the quality of the numerical fitting and to allow time for the fitting. The dead time and the low signal amplitude at “shoulders” of the frequency characteristics, which constitute the majority of the measurement phase, also sacrifice the signal-to-noise ratio. To achieve acceptable noise in practice after accounting for these requirements, it is difficult to lower the time per measurement, which comprises the data acquisition time and the fitting time, below 500 ms with most current impedance analysers [30]. Seiko has commercialised a fast impedance analyser for electrochemical quartz resonators with a minimum time per measurement of 100 ms [31]. However, there is no reported data on noise at this speed with real experiments.

In ring-down analysis method, commonly referred to as quartz crystal microbalance with dissipation monitoring (QCM-D), a QCR is excited with a narrow radio frequency pulse comprising a frequency somewhat closer to the resonance frequency. The excitation is

* Corresponding author. Tel.: +44 (0)1509 227692.
E-mail address: S.Ghosh2@lboro.ac.uk (S.K. Ghosh).

https://doi.org/10.1016/j.snb.2018.11.052
Received 14 March 2018; Received in revised form 2 November 2018; Accepted 9 November 2018
Available online 13 November 2018

intermittently turned off and the transient signal (voltage or current) from the QCR is fitted with an exponentially decaying (or 'ringing down') sinusoidal signal to extract the resonance frequency and dissipation. One may apply averaging for better accuracy of fitting at the cost of increased measurement time. Moreover, like the impedance analysis method, here too the data acquisition dead time between successive ring-downs and the low signal amplitude during majority of the measurement phase sacrifice the time resolution and the signal-to-noise ratio. Accounting for these requirements, Petri, Johannsmann and co-workers reported the minimum time per measurement for ring-down analysis method to be in the range of 1 s to achieve acceptable noise in practice [30]. Q-Sense E1 reports a minimum time resolution of 5 ms for their 5 MHz QCRs, which employ the ring-down or QCM-D method [32]. However, there is no reported data demonstrating the noise at this speed. The noise is normally predominantly from the bio-functionalised surface. A study of glycoprotein–lectin interactions using QCM-D reported a 2 Hz noise of frequency measurement [33].

In oscillator circuits, the resonance frequency of a QCR is actively interrogated using a frequency counter and averaged over a particular time interval. The dissipation factor is estimated using an automatic gain control unit within the oscillator circuit, which compensates the acoustic energy loss through a feedback circuit to maintain a constant amplitude of the QCR without altering its quality factor. Oscillator circuits usually have a time resolution of 1 s [34,35]. It is possible to achieve a higher time resolution using reciprocal frequency counters with high reference clock frequency [34] albeit at the expense of complexity in instrumentation. The theoretical noise or frequency resolution, Δf, with a reciprocal frequency counter is related with the time resolution, t, by the equation $\Delta f = f_q/(f_{rec}\,t)$, where f_q is the QCR fundamental resonance frequency and f_{rec} is the reference clock frequency [36]. According to this equation, in principle one could achieve a time resolution of 100 ms with a noise of 0.14 Hz using a 1 GHz reciprocal frequency counter on a 14.3 MHz QCR, which is the one employed in our current work. However, in practice there are various other kinds of noise associated with liquid, e.g. signal's phase jitter, and predominantly with a bio-functionalised QCR, which makes it challenging to go below 1 s time resolution. There isn't any experimental evidence of less than 1 s time resolution with a QCR using frequency counters.

To circumvent the speed of measurement problem, Petri, Johannsmann and co-workers presented a method, where fast time traces of electrical admittance were acquired sequentially at a set of fixed frequencies closely around the resonance frequency, and subsequently fitted them to obtain resonance frequency and dissipation [30]. They reported a minimum time per measurement of 10 ms and noise of 0.3 Hz for copper deposition/dissolution with data gathered over 7 min. However, these measurements are only valid over a span that is much smaller than the resonance bandwidth as they use a linear approximation function. Moreover, the frequency characteristics are required to be taken for every new QCR to determine the local slope and intercept of the linear approximation before this method can be applied. Importantly, this method is applicable only for studying repetitive processes, such as in electrochemistry. In nature, there are 'single-shot' quick or transient processes, often requiring shorter time period of measurement than 10 ms. For example, gas-to-surface adsorption-desorption dynamics in surface science [37], formation of chemical reaction intermediates and important biomolecular events, such as protein folding [38] or other structural changes during binding, are non-repetitive processes occurring in millisecond timescales. Studying these fast transient processes is critical to their phenomenological or mechanistic understanding.

In this paper, we report a new method for measuring the resonance frequency and dissipation of a mechanical oscillator based on their analytical expressions derived using the Butterworth-Van Dyke equivalent electrical circuit model. These expressions allow the estimation of resonance frequency and dissipation using simple instrumentation directly and continuously from each impedance datapoint acquired from a fixed amplitude and frequency of drive without any fitting or measurement dead time. Consequently, the time resolution is practically limited by the duration of transient processes on the oscillator or the digital data acquisition time period of the instrument, whichever is higher. The absence of dead time and of low-amplitude data acquisition and the feasibility of analog or digital signal averaging of the linear impedance signal for any desired time allow an ultra-low noise from the method. We have referred to this method of determination of resonance frequency and dissipation as 'fixed frequency drive' or FFD.

An analytical model is presented along with experimental validations for inertial and viscous loading on a 14.3 MHz QCR. The shifts in resonance frequency and dissipation obtained from streptavidin-biotin binding and from replacement of methanol with deionised water on the QCR using FFD method compared closely with those obtained from impedance analysis method using the same instrumentation. A study of quick needle touches on a QCR functionalised with a thiol self-assembled monolayer is also reported. The realtime resonance frequency shift features associated with the transient loading and unloading of the needle on the QCR in liquid could be detected with a minimum time resolution of 112 μs, which is nearly two orders of magnitude lower than that reported by Petri and co-workers. A study of baseline noise of a thiolated QCR in liquid using FFD for a wide range of measurement time period (time to record one data point) from 33 μs to 42 s is presented and the noise data is comparatively discussed with other methods. The potential for greater multiplexability and implementability on a single silicon chip are also discussed.

2. Theory

The dynamics of an oscillator around a resonance mode can be presented in the form of a spring-mass-damper model (Fig. 1a). The equivalent electrical circuit for this dynamic model is given by an RLC circuit, where the electrical resistance (R), inductance (L), capacitance (C) and charge (q) are related to the coefficient of damping (c), mass (m), stiffness (k) and displacement (x) respectively as $R = c$, $L = m$, $C = 1/k$ and $q = x$. For a quartz crystal resonator, the equivalent electrical circuit is given by the Butterworth-Van Dyke (BVD) model (Fig. 1b), where the branch containing R_m, L_m and C_m models the oscillator dynamics and is often referred to as the motional branch, and the shunt capacitance (C_0) models the dielectric capacitance of the quartz and any holder capacitance [28].

From the BVD model, the impedance of the motional branch is given by

$$Z_m = R + j\omega L - \frac{j}{\omega C} \tag{1}$$

where $\omega = 2\pi f$ is the drive frequency in rad/s. At resonance (when $\omega = \omega_0$), the motional impedance is purely resistive, which means the motional reactance (or the imaginary component of impedance), given by $j(\omega L - \frac{1}{\omega C})$, is zero. This gives the resonance frequency ($\omega_0 = 2\pi f_0$) of the motional branch as

$$\omega_0 = \frac{1}{\sqrt{LC}} = \frac{\rho}{L} = \frac{1}{\rho C} \tag{2}$$

where $\rho = \sqrt{L/C}$ is the characteristic impedance. From Eq. (2), we have

$$L = \frac{\rho}{\omega_0} \tag{3}$$

$$C = \frac{1}{\rho\omega_0} \tag{4}$$

Using Eqs. (3) and (4) to substitute for L and C in Eq. (1), we have

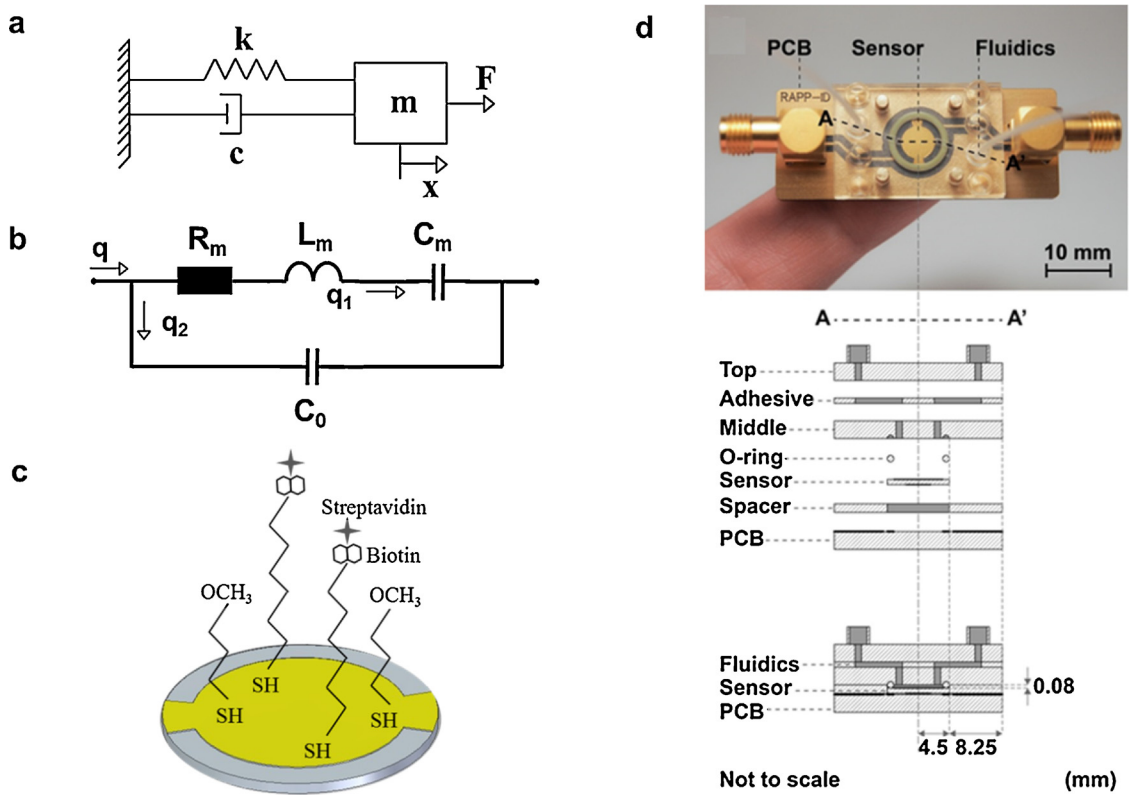

Fig. 1. a. Spring-mass-damper model of a resonance mode of an oscillator. **b.** Butterworth-Van Dyke (BVD) model of a quartz crystal resonator (QCR). **c.** Streptavidin binding to biotin-thiol functionalised on a QCR. **d.** Assembly of a QCR between the microfluidic cartridge and a PCB.

$$Z_m = R + j\rho\left(\frac{\omega}{\omega_0} - \frac{\omega_0}{\omega}\right) \tag{5}$$

$$\Rightarrow Z_m = R + j\rho\left(\frac{f}{f_0} - \frac{f_0}{f}\right) \tag{6}$$

From Eq. (6) the motional reactance can be expressed as

$$X_m = \rho\left(\frac{f}{f_0} - \frac{f_0}{f}\right) \tag{7}$$

Solving Eq. (7) for f_0, we have

$$\rho f_0^2 + X_m f f_0 - \rho f^2 = 0 \tag{8}$$

$$\Rightarrow f_0 = \frac{f}{2\rho}(-X_m + \sqrt{X_m^2 + 4\rho^2}) \tag{9}$$

Eq. (9) gives the expression for resonance frequency of an oscillator in terms of the drive frequency, the motional reactance and the characteristic impedance of the equivalent electrical circuit. It may be noted that the impedance measured from an experiment is the equivalent impedance, which takes into account the impedance due to the shunt capacitance (C_0) as modelled by the BVD equivalent circuit (Fig. 1b), and is given by $Z = \left(\frac{1}{Z_m} + j\omega C_0\right)^{-1}$. The impedance of the motional arm is obtained from this experimentally measured equivalent impedance as $Z_m = (1/Z - j\omega C_0)^{-1}$, and $X_m = Im(Z_m)$ is used in Eq. (9).

Using Eq. (9), the frequency offset, i.e. the difference of the resonance frequency with respect to the drive frequency (Δf_{off}), is expressed as

$$\Delta f_{off} = f_0 - f = \frac{-f}{2\rho}(X_m + 2\rho - \sqrt{X_m^2 + 4\rho^2})$$

The above equation can be alternatively expressed as follows after eliminating larger values inside the bracket.

$$\Delta f_{off} = -f\frac{X_m}{2\rho}\left(1 - \frac{\frac{X_m}{2\rho}}{1 + \sqrt{1 + \left(\frac{X_m}{2\rho}\right)^2}}\right) \tag{10}$$

Mass or elastic loading on the oscillator due to any process on the surface modifies the inductance or capacitance of the equivalent circuit respectively, and hence, shifts the resonance frequency ($\omega_0 = 2\pi f_0$) governed by Eq. (2). If the oscillator is driven at a known fixed frequency f, then the resonance frequency or its offset from the drive frequency at any point during the process can be determined using Eq. (9) or Eq. (10) respectively. This allows the measurement of resonance frequency shift from each impedance datapoint directly.

2.1. Shunt capacitance and characteristic impedance

The shunt capacitance (C_0) and the characteristic impedance (ρ) are nearly the same for any crystal in a batch. The representative values for a batch can be either obtained from the manufacturer or determined by an impedance analyser. The coefficient of variation of C_0 and ρ for 6 randomly chosen crystals from our batch was 3.3% and 0.9% respectively. This amount of variation has no practical impact on the estimations using FFD method (Eq. (9) or Eq. (10)). Although the characteristic impedance changes slightly with any shift in resonance frequency during a process, it can be assumed to be practically constant without any notable impact on the accuracy of estimation of the resonance frequency shift using Eq. (10). The analytical justification for this is provided in Supplementary information §S1.

2.2. Choice of drive frequency

The driving frequency does not need to be close to the resonance frequency for accurate estimation of the latter from Eq. (9) or Eq. (10). In principle, the drive frequency can be several resonance bandwidths

away from the drive frequency without practically affecting the accuracy of estimation. Our estimated range for driving frequency selection is roughly ± 20 kHz (Supplementary information Fig. S2), which for the crystals used in this study is around 5.6 resonance half-bandwidths away for operation in liquid ($Q \sim 2000$, $\Rightarrow \frac{\gamma}{2} = \frac{\omega_0}{2Q} = 3.57\,kHz$, where $\gamma = c/m$), and more than 150 half-bandwidths for operation in air ($Q > 50000$). However, for better signal-to-noise ratio, it would be useful to choose the nominal resonance frequency of the batch of crystals obtained from the manufacturer as the drive frequency. With most manufacturers, the frequency tolerance is ± 100 ppm or better, i.e. the maximum difference between the resonance frequency of any crystal in a batch and the nominal resonance frequency of the batch is ± 100 ppm or less. For our 14.3 MHz from Laptech Precision Inc., the frequency tolerance is ± 1.5 kHz (~100 ppm), which is well within the resonance half-bandwidth in liquid (3.57 kHz). The frequency tolerance can also be as low as 10 ppm at slightly higher cost. Hence, the drive frequency set to the batch's nominal frequency should ensure both accuracy and good signal-to-noise ratio.

It may be noted that the second order Maclaurin series approximation of the frequency offset in Eq. (10), as shown in Eq. (11), gives an error of only ~7 μHz with respect to the exact expression for a resonance frequency shift of up to ~20 kHz, i.e. 5.6 resonance half-bandwidths in liquid for the QCR used in this study (Supplementary information §S2). Thus, the approximate form as in Eq. (11) can be used in place of the exact expression of Eq. (10) for all practical purposes. Moreover, the simpler formula obviates the need for calculation of radicals and potentially allows the use of a simple and cheap microprocessor.

$$\Delta f_{off} = -f\alpha\left(1 - \frac{\alpha}{2}\right);\ \alpha = \frac{X_m}{2\rho} \tag{11}$$

2.3. Dissipation shifts using FFD

In the electrical equivalent, the quality factor is given by $Q = \rho/R$ (Supplementary information §S3). The dissipation factor is therefore measured as follows.

$$D = 1/Q = R/\rho$$

$$\Rightarrow D = Re(Z_m)/\rho \tag{12}$$

Hence, the dissipation and its change over a process can be derived directly from Eq. (12) using the motional resistance (real part of motional impedance) measured during a fixed frequency drive.

3. Quantitative validations with impedance analysis method

Resonance frequency and dissipation shifts derived using the FFD method (Eqs. (11) and (12)) were validated against the respective values derived using the impedance analysis method through two types of experiments: streptavidin binding to biotin immobilised on the QCR, and replacing methanol with deionised (DI) water on the QCR. While the former is predominantly an inertial (or mass) loading experiment, causing shifts in resonance frequency, the latter is a combination of both inertial and viscous loading (due to changes in density and viscosity of the coupled liquid), causing shifts in both resonance frequency and dissipation.

3.1. Streptavidin-biotin binding

14.3 MHz AT-cut thickness-shear-mode QCRs were functionalised with a self-assembled monolayer of mixed thiol (10% biotin thiol, 90% methoxy thiol) (Fig. 1c) and assembled between a microfluidic flow cell, made of cyclic olefin copolymer, to allow a controlled delivery of sample, and a printed circuit board to enable the electrical connection (Fig. 1d). The QCR was actuated and sensed electrically using a dedicated network analyser, designed and built in-house, and reported in our earlier work [39]. The details of the set-up and processes are provided in the **Materials and methods** section.

Frequency sweeps (0.1 s, 0.52 V, span = 20 kHz) and fixed frequency scans (0.1 s, 0.52 V) were taken using the above-mentioned network analyser successively every 2 min in phosphate buffer saline (PBS) to establish a baseline for 10 min. 2.5 μg/mL streptavidin solution in PBS was then injected (at 40 μL/min) into the microfluidic cell to allow binding for 10 min. After this binding phase, similar frequency sweeps and fixed frequency scans as above were taken for 10 min.

For the impedance analysis method, the resonance frequency ($\omega_0 = 2\pi f_0 = 1/\sqrt{LC}$), the quality factor ($Q = \sqrt{L/C}/R$), the shunt capacitance (C_0) and the characteristic impedance ($\rho = \sqrt{L/C}$) were estimated from each frequency sweep by fitting the measured impedance with the equivalent impedance from the BVD model (Fig. 1b). The shunt capacitance and the characteristic impedance estimated at the beginning of the experiment were used in the fixed frequency drive (FFD) method through the baseline and binding measurement phases.

To study the dependence of the resonance frequency estimate from the FFD method on the choice of drive frequency, fixed frequency scans were taken at 5 different drive different frequencies spanning ~84% of the frequency bandwidth: $f_{0,PBS}$ − 3 kHz, $f_{0,PBS}$ − 1.5 kHz, $f_{0,PBS}$, $f_{0,PBS}$ + 1.5 kHz and $f_{0,PBS}$ + 3 kHz, where $f_{0,PBS}$ is the resonance frequency of the QCR in PBS at the beginning of the experiment. The calibrated reactance of the motional branch (X_m) from each fixed frequency scan was used to estimate the resonance frequency and dissipation according to Eqs. (11) and (12) respectively. In addition, each drive frequency point in a frequency sweep of 20 kHz span was used to estimate the resonance frequency and dissipation according to the FFD method and averaged. All of the above 6 estimates from the FFD method were compared with that from the impedance analysis method.

The shifts estimated from the FFD and impedance analysis methods at each measurement point showed satisfactory agreement over the baseline and streptavidin-bound phases for all the 5 drive frequencies (Fig. 2a). The resonance frequency shifts due to streptavidin-biotin binding estimated from these two methods also showed satisfactory agreement (Fig. 2b). The agreement varied between +8.16% (SD, σ= 2.98%) and -4.33% (SD, σ= 3.66%) over the range of drive frequencies explored, and was found to be the most satisfactory at +0.16% (SD, σ= 2.12%) when the drive frequency for FFD was set to $f_{0,PBS}$ (Fig. 2c). While this agreement is already reasonably good for practice, it can be improved further through a more accurate calibration and potential improvement to the model of equivalent electrical circuit of the QCR through the consideration of shunt resistance and electrode resistance [40].

The experimentally measured frequency shift values from both impedance analysis and FFD methods agreed reasonably well (within 37%) with the theoretical frequency shift (−230 Hz) estimated using the Sauerbrey equation [41] (Supplementary information §S4).

The dissipation shifts were also derived experimentally using the impedance analysis and FFD methods from the admittance curve fitting and Eq. (12) respectively. The fractional shifts in dissipation due to the binding event ($\Delta D/D$) measured from the impedance analysis method (+0.002) was in close agreement with those measured from FFD method (+0.005 to -0.007) for the various drive frequencies explored (Fig. 2a). The percentage agreement was not assessed as the dissipation values were small.

3.2. Methanol-DI water replacement

Experiments were also carried out with cleaned unfunctionalised QCR, where methanol (MeOH) in the sample chamber above the QCR was replaced with deionised (DI) water. The changes in resonance frequency and dissipation resulting from the changes in mass and viscous loading were measured using the impedance analysis and FFD methods and compared.

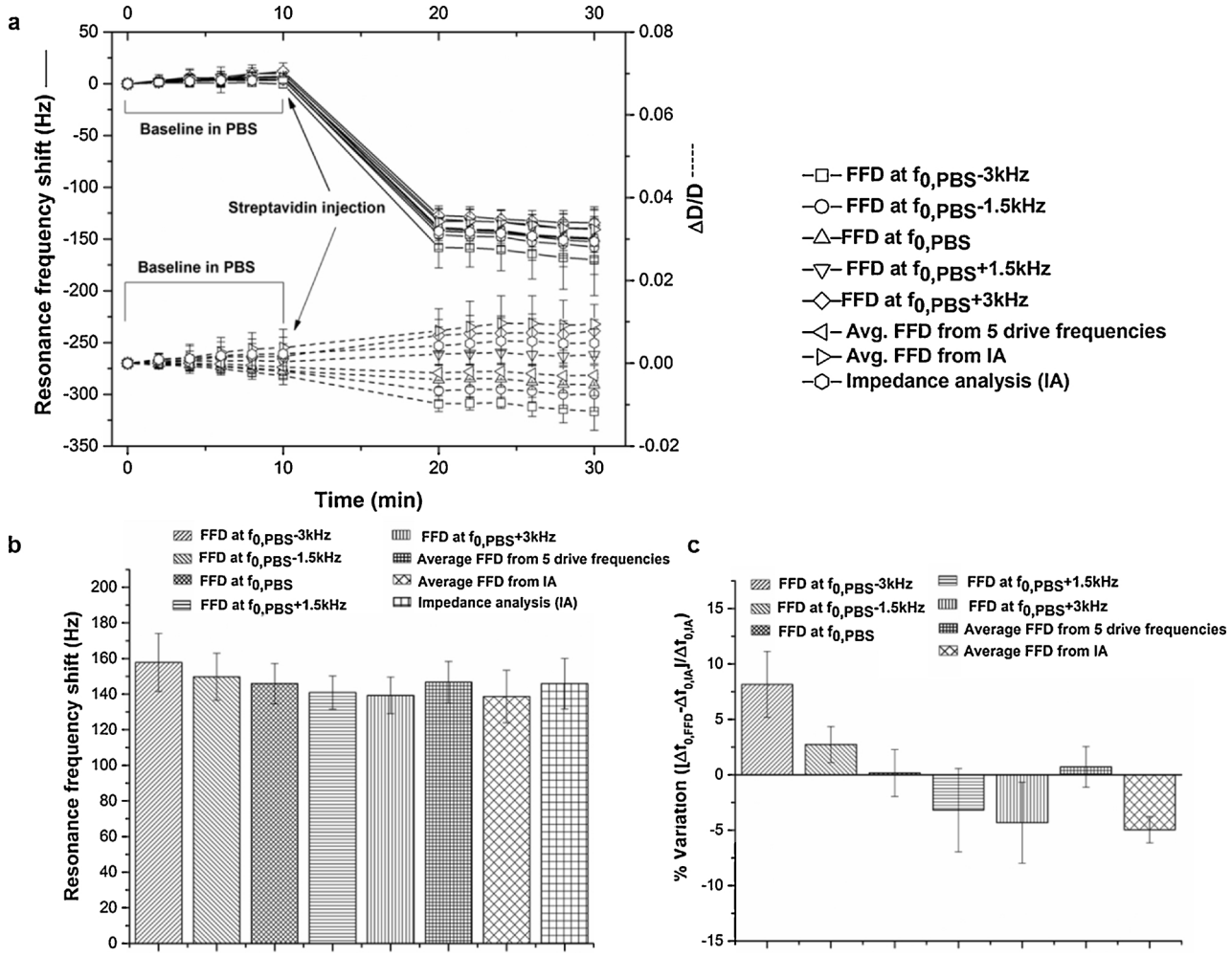

Fig. 2. a. Resonance frequency and relative dissipation shifts due to streptavidin binding using impedance analysis and FFD methods (with 5 drive frequencies) with 2 min measurement interval **b.** Resonance frequency shift 10 min after streptavidin injection. **c.** Percentage variation in resonance frequency shifts for FFD (at different drive frequencies) with respect to impedance analysis method.

Frequency sweeps and fixed frequency scans at a range of drive frequencies were recorded in a similar way as in the streptavidin-biotin binding experiment described in Section 3.1. Likewise, the frequency sweeps were analysed using the impedance analysis method (BVD model fitting) and the fixed frequency scans were analysed using the FFD method (Eqs. (11) and (12)) to determine the resonance frequency and dissipation shifts due to the replacement of methanol with DI water. This time, the sets of measurements were repeated every 5 min during the 20-minute baseline phase in methanol and during the 20-minute phase in DI water.

The resonance frequency and dissipation shifts estimated from the impedance analysis and FFD methods at each measurement point showed satisfactory agreement over both the methanol baseline phase and the DI water phase for all 5 FFD drive frequencies (Fig. 3a, b, d). The agreement in the resonance frequency shifts varied between +2.8% (SD, σ= 0.89%) and -0.25% (SD, σ= 0.68%) over the range of FFD drive frequencies explored, and was found the most satisfactory 0.67% (SD, σ= 0.66%) when the drive frequency was set to $f_{0,\mathrm{MeOH}} - 1.5$ kHz, where $f_{0,\mathrm{MeOH}}$ is the resonance frequency of the QCR in methanol measured at the beginning of the experiment using impedance analysis (Fig. 3c). The agreement in the fractional shifts in the dissipation factor ($\Delta D/D$) varied between -10.9% (SD, σ= 1.42%) and +4.67% (SD, σ= 1.59%) over the range of FFD drive frequencies explored, and was found to be the most satisfactory 1.58% (SD, σ= 0.7%) when the drive frequency for FFD was set to $f_{0,\mathrm{MeOH}} + 1.5$ MHz (Fig. 3e).

The experimental values of resonance frequency and dissipation shifts from both the methods were in good agreement with the respective theoretically estimated values using the Kanazawa's equation (Supplementary information §S5). The theoretically estimated resonance frequency shift (−995 Hz) was within 0.92% of the value measured using the impedance analysis method and +0.67% of the value measured using the FFD method with the drive frequency set to $f_{0,\mathrm{MeOH}}$. Similarly, the theoretically estimated fractional shift in the dissipation factor (0.438) was within 0.76% of the value measured using the impedance analysis method and -1.96% of the value measured using the FFD method with the drive frequency set to $f_{0,\mathrm{MeOH}}$.

4. Noise analysis

The instrument, the method and the random processes on the sensor surface are the major sources of noise in a bioanalytical measurement. In particular, the processes on the surface dominate the noise in biosensors. For a given instrument and surface, the noise due to the method relies closely on the data acquisition rate, with the noise usually increasing with faster data acquisition. Studies related to baseline noise over various data acquisition rates for a given instrument and sensor surface are missing in the QCR literature.

In this work, a continuous fixed frequency scan (0.47 V, 100 s) was acquired from a QCR functionalised with a self-assembled monolayer of

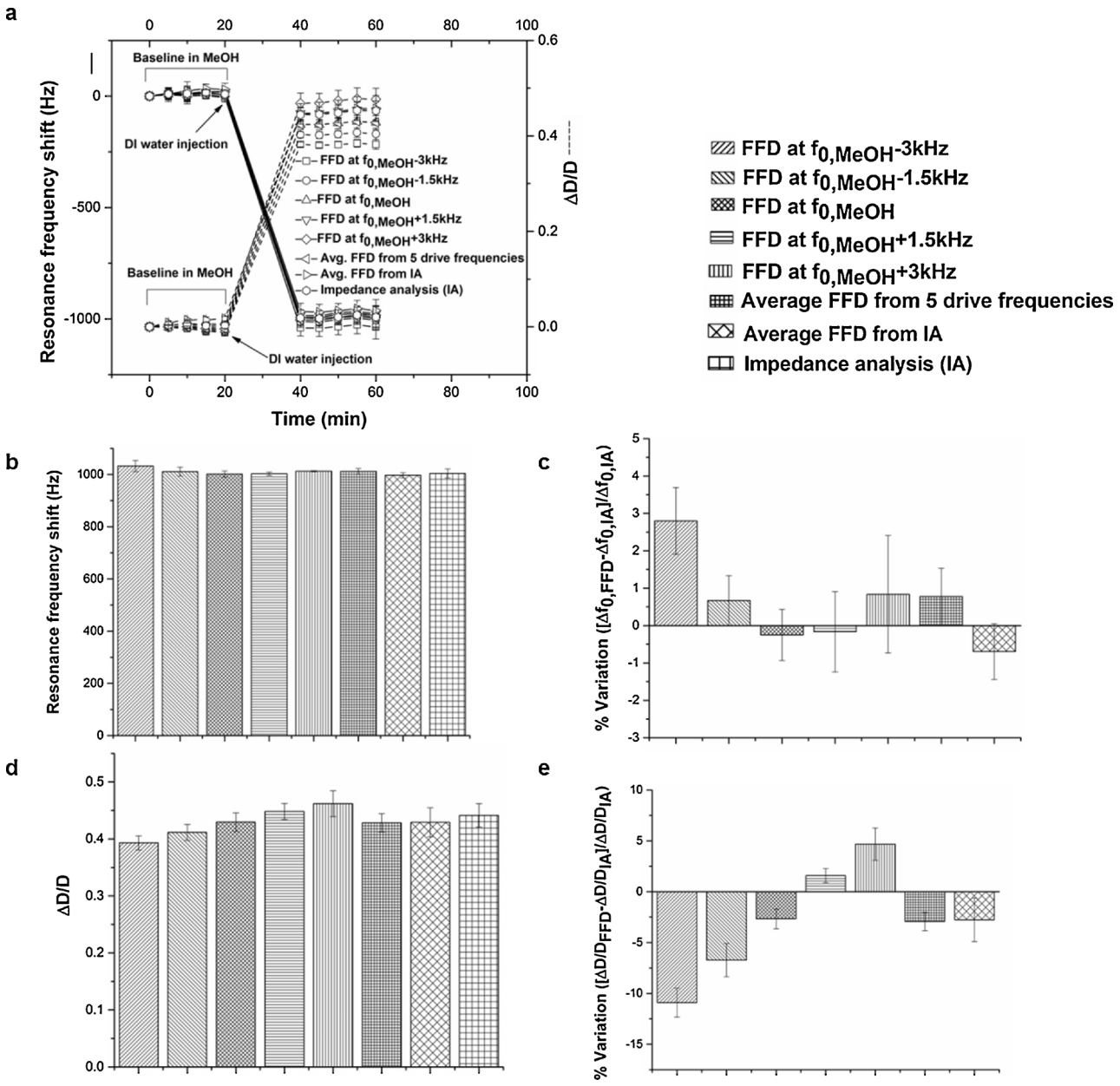

Fig. 3. a. Resonance frequency and relative dissipation shifts due to change in liquid phase from methanol to DI water using the impedance analysis and FFD methods (with 5 drive frequencies) with 5 min measurement interval **b.** Resonance frequency shift 20 min after flow of DI water. **c.** Percentage variation in the resonance frequency shifts for FFD (at different drive frequencies) with respect to impedance analysis method. **d.** Relative dissipation shift 20 min after flow of DI water. **e.** Percentage variation in the relative dissipation shift for FFD (at different drive frequencies) with respect to impedance analysis method.

thiol in PBS at a data acquisition time period of 32.76 μs employing the afore-mentioned custom-built network analyser. Exponential running averages were then applied on this linear data in order to obtain data streams corresponding to a range of acquisition time periods from 32.76 μs to 41.89 s. This ensured that the data streams for all the time periods were associated with the same time, duration and state of the sensor surface. For each data stream, the resonance frequency was determined for every impedance data point using the FFD method (Eq. (11)) and the Allan deviation noise was evaluated. Fig. 4 and Table 1 show the Allan deviation noise corresponding to each data acquisition time period [42].

An Allan deviation noise of 1 Hz or less was recorded for data acquisition time periods of 2 ms or higher (Table 1, Fig. 4). A practical noise performance such as this with a functionalised 14.3 MHz QCR in liquid at ~millisecond time period of data acquisition is encouraging and not encountered before in the QCR literature. Moreover, this noise was achieved over a sampling period of 100 s only, which is a few times shorter than the copper deposition/dissolution sampling period (7 min) by Petri, Johannsmann and co-workers, who reported a minimum time per measurement of 10 ms (noise ~0.3 Hz with 5 MHz QCR) [30]. An Allan deviation noise of 4.7 Hz was recorded at the smallest data acquisition time period of 32.76 μs. While 4.7 Hz is not a low noise in general, it is still encouraging for a functionalised QCR in liquid given this high speed of data acquisition. For comparision, one may note that even the theoretical digital noise for a 14.3 MHz QCR with a 1 GHz reciprocal frequency counter is 436 Hz at a similar acquisition speed [36].

It may be noted that the above noise performance of the FFD method was with a thiol-functionalised 14.3 MHz QCR in liquid. The noise purely from the instrument was much lower even over a shorter sampling period. We modelled the load under liquid with a 180 Ω resistor in series with an encapsulated 14.3 MHz QCR. The baseline

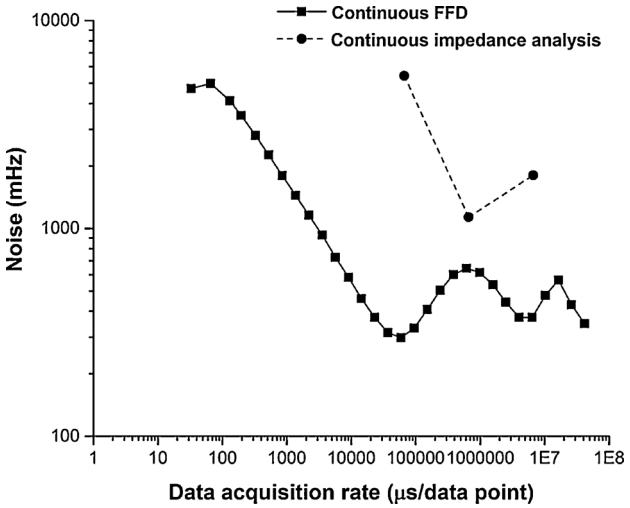

Fig. 4. Allan deviation noise estimated from continuous fixed frequency drive (FFD) and continuous impedance analysis methods at various data acquisition time per measurement.

Table 1
Allan deviation baseline noise in PBS for Fixed Frequency Drive (FFD) and Impedance Analysis methods over various data acquisition speeds, and noise comparision at comparable speeds.

Fixed Frequency Drive (FFD)		Impedance Analysis		Noise ratio (FFD/Imp. Analysis)
Data acquisition time period (ms)	Allan deviation noise (Hz)	Data acquisition time period (ms)/ Measurement time period (ms)	Allan deviation noise (Hz)	
0.033	4.71			
0.066	4.99			
0.131	4.11			
0.197	3.50			
0.328	2.80			
0.524	2.26			
0.852	1.80			
1.376	1.44			
2.195	1.16			
3.539	0.93			
5.669	0.73			
9.077	0.58			
14.483	0.46			
23.167	0.37			
37.028	0.32			
59.179	0.30	66.5/800	5.43	0.055
94.568	0.33			
151.159	0.41			
241.533	0.51			
385.942	0.60			
616.727	0.64	665/1250	1.13	0.567
985.498	0.61			
1574.730	0.54			
2516.290	0.44			
4020.860	0.37			
6425.020	0.37	6650/7690	1.80	0.207
10266.700	0.48			
16405.300	0.56			
26214.400	0.43			
41888.500	0.35			

frequency fluctuation (Allan deviation noise) of this device measured using FFD in our instrument at a data acquisition time period of 8.4 ms and over a sampling period of 400 ms was ~0.15 Hz (Supplementary information Fig. S4). The noise fitted well with the theoretical curve for the additive normal 'white' noise that reduced reciprocally to the square root of the sampling period.

4.1. Noise comparision with impedance analysis method

Continuous frequency sweeps (0.03 V, 100 s) were also acquired for the same thiol-functionalised QCR in PBS by employing a commercial bench-top Vector Network Analyzer (VNWA 3E, SDR-Kits, UK) at three data acquisition time periods available with the instrument: 66.5 ms, 665 ms and 6650 ms. The admittance data was fitted internally by the instrument software to deliver the resonance frequency baseline based on the impedance analysis method for these three time periods. The Allan deviation noise was determined and compared with those from the FFD method for the three comparable data acquisition time periods (Fig. 4, Table 1). We had to employ a different instrument to do the noise study for the impedance analysis method as the lowest time period for frequency sweep impedance analysis with our custom-built network analyser is ~1 s. It may be noted that the measurement time periods with the VNWA 3E analyser are larger than the above-mentioned data acquisition time periods to accommodate for the time to fit the impedance data (Table 1). We have compared the noise of the two methods based on the data acquisition time periods so that the comparision is as close as possible between the methods alone and not influenced by the speed of the fitting algorithm or processor.

The noise values obtained from the continuous FFD method were considerably lower at similar data acquisitions speeds, e.g. the noise from the FFD method was 5.5% of the noise from the impedance analysis method at an acquisition time period of ~66.5 ms (Fig. 4, Table 1). Although differences in the two instruments used (e.g. receivers and analog-to-digital converters) could influence the difference in noise observed, we believe the difference in the methods of resonance frequency measurement played a crucial role because of the following arguments. For the impedance analysis method, the impedance data was collected across a range of frequencies encompassing the resonance bandwidth - the lower signal-to-noise ratio for frequencies away from resonance could impact the quality of fitting. There was also a data acquisition dead time required for fitting the data. Moreover, the resonance characteristics fitting is nonlinear, where the noise does not average to zero, causing random offset in the fitting parameters, such as the resonance frequency. In comparison, the impedance data in the FFD method was collected at a fixed amplitude and at a single frequency near the resonance frequency. There was no fitting needed, hence, no data acquisition dead time. Furthermore, the fixed amplitude data could be easily averaged over the entire acquisition period using a linear running average function, where the noise averages statistically to zero.

We would like to put forward another hypothesis behind lower noise with the FFD method. In the impedance analysis and the ring-down methods, the oscillation amplitude of the QCR varies over a scan with near-zero amplitude during a significant proportion of a measurement cycle to eliminate the transient interference and allow time for numerical fitting. So it is likely that any loosely-bound micro- or nanoparticle "debris" that settle down on the functionalised surface during the low-amplitude phase through weak electrostatic bonds are chaotically dislodged during the higher-amplitude phase of the scan. Dislodging can occur due to combined chaotic thermal-assisted molecular motion and mechanical forces of the oscillation. The randomness of the lodging/dislodging of these particles on the QCR surface could be a major contributor to noise. These random attachments/detachments of loosely-bound particles are much reduced in the FFD method as the amplitude of motion is constant. Weakly interacting particles are less likely to settle down in the first place on constantly oscillating surface. This is the reason why such component of noise in the FFD method is drastically reduced.

5. Time resolution of frequency shift measurement

The time resolution is governed by both the minimum data acquisition time period and the duration of transient oscillations in the QCR,

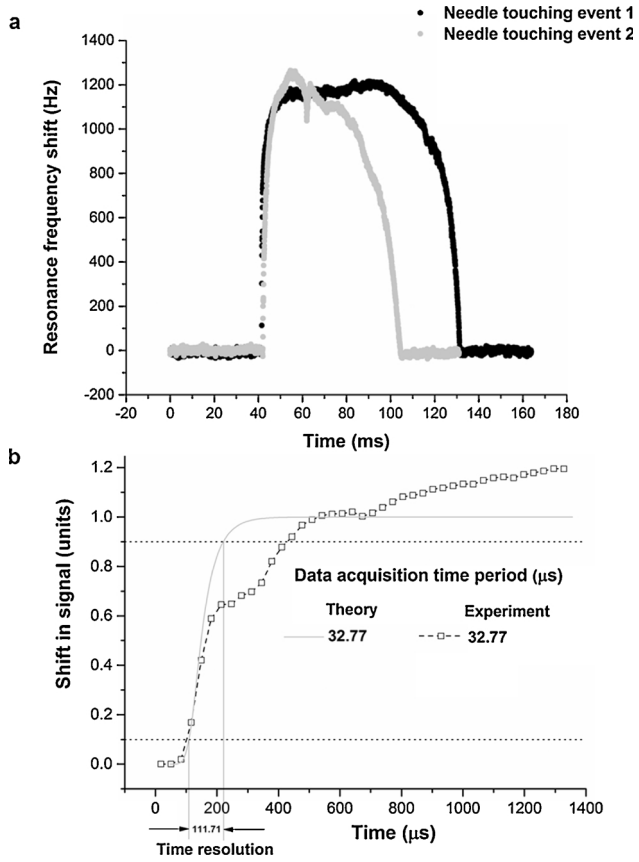

Fig. 5. a. Resonance frequency shift measured from two successive needle touches with a data acquisition time period of 32.7 μs. **b.** The time period of the first frequency rise feature in a representative needle touch experiment recorded over the initial 1.4 ms compared well with the theoretically estimated front rise time of a step change in signal amplitude.

particularly whichever is higher. In our 14.3 MHz QCR, the duration of transient oscillations, given by $2Q/\omega_0$, where Q is the quality factor and ω_0 is the fundamental resonance frequency in rad/s, is ~44.5 μs whereas the digital data acquisition time period for our instrument is ~32.7 μs. Since these time periods are close to each other, the time resolution of measurements is influenced by both.

To study the time resolution of frequency shift measurement, we conducted quick needle touch experiments on a biotin thiol functionalised QCR in PBS. Jumps in the resonance frequency were observed at the moments of needle touches that were measured using the FFD method. These jumps could be justified because during the touch, while the tip of the metallic needle touching the QCR moved with the surface, the rest of the needle remained nearly stationary. As a result, the needle acted as an additional 'spring' or elastic restoring force, causing the increase in resonance frequency.

The frequency rise and decay features in timescales of 60–90 ms were clearly distinguishable using a continuous scan of fixed frequency and amplitude. Fig. 5a shows two representative needle touch events measured using the FFD method. We were unable to detect these needle touches with this distinction using the Vector Network Analyzer from SDR-Kits that applies the impedance analysis method (Supplementary information Fig. S3). Although this instrument allowed a minimum data acquisition time period of 66.5 ms, the measurement time period including the processing time was 800 ms.

To validate the experimental observation, we theoretically estimated the front rise time, i.e. the time between 10% and 90% of a step value, for a recorded signal due to a stepwise transient process on a QCR with a quality factor of 2000 and a 30.5 kHz receiver (Supplementary information §S8). The theoretically estimated rise time for the quickest data acquisition time period (32.77 μs) was found to be ~112 μs, which agreed quite well with the duration of the "first frequency rise feature" of a representative needle touch experiment (Fig. 5b). We therefore define this time period as the time resolution of the method using the current QCR and the instrument.

6. Discussion

Measurement of multiple parameters is of wide interest in diagnostics, drug development and biomarker analysis. However, the degree of multiplexability with QCRs has been limited as electromagnetic coupling is usually eliminated with expensive shielding. Moreover, although single-chip integration of QCR measurements would allow low cost-per-unit through economies at scale, the high costs involved with the current complexity are apparently prohibitive. Being an analytical formula-based method operating at a fixed frequency and requiring no numerical fitting, the FFD method offers some unique potential for a greater degree of multiplexability and single-chip integration as discussed below. These capabilities are worth exploring experimentally through future work.

6.1. FFD with self-oscillator quartz as a generator – potential for high multiplexability

In one embodiment, it is possible to implement the FFD method with one quartz resonator in a self-oscillating mode, such as an oscillator circuit, serving as a generator of fixed frequency for another quartz resonator acting as the sensor. Both the QCRs can be from the same batch and exposed to the same liquid in order to provide the best compensation for temperature and other factors, such as viscosity. This embodiment would be simple, potentially low-cost and, with no need for fitting unlike the ring-down or the impedance analysis methods, favour a greater degree of multiplexability of QCRs.

Currently, for multiplexed detection, multiple QCR sensors are often fabricated on a single piece of quartz substrate [33,43–56]. Such a sensor is termed as multi-channel monolithic quartz crystal microbalance (MQCM). In traditional methods, all QCRs can be driven in parallel mode by using a separate driver circuit, such as an oscillator, pulse generator or frequency synthesizer, for each QCR and then capturing the output signal from each and processing it using a central processing unit. This makes the integrated electronic circuit bulky. Alternatively, the QCRs can also be driven in time multiplexing mode using electronic switches at the cost of complexity of the circuit and sacrificing the time resolution and noise of measurement. In both these modes of drive, the complexity and spurious electromagnetic coupling limits the degree of multiplexability. In the FFD method, all sensor QCRs (passive) can be driven simultaneously by using a single self-oscillating QCR (active), which forms a part of an automatic gain controlled oscillator circuit devoid of frequency counter. The simplicity in this embodiment potentially favours a greater degree of multiplexability.

MQCMs are affected by acoustic and electromagnetic couplings among adjacent QCRs. Acoustic coupling in any method can be suppressed by using inverted mesa quartz substrate [55], insertion of polydimethylsiloxane or other acoustic dissipation wall between QCR sites positioned on a single quartz [55] and maintaining a certain distance between the QCRs [54], to name a few. However, electromagnetic coupling between the metal electrodes [52], transmission lines and fluidic channels [55] of the QCRs is either very hard to eliminate or too expensive to do so by the use of shielding. To deal with spurious electromagnetic couplings between the QCRs, impedance analysis and FFD methods can be calibrated in principle by obtaining a matrix of cross-coupling coefficients and then using it to eliminate cross-interference to a high degree, relaxing requirements for design complexity and cost, such as with shielding. Calibration in the impedance analysis method is relatively more cumbersome as the MQCM device needs to be

calibrated at each and every frequency of a certain frequency sweep, whereas in the FFD method, calibration at a single frequency, such as the QCR resonance frequency, can address the requirement. Cancelling electromagnetic coupling is problematic in ring-down method due to the absence of any defined calibration and fitting procedure in presence of electromagnetic coupling. Hence, multiplexability requires expensive shielding, which limits the degree of multiplexability.

6.2. Potential for single-chip integration

The design of FFD integration on a single chip substrate is potentially less expensive and consumes less power than that for impedance analysis and ring-down methods. This is because with no need for frequency synthesizers or fast analog-to-digital converters with a large dynamic range, FFD needs a chip with a much lower degree of integration. Single-chip integration can reduce the cost per unit due to economies of scale and significantly expand the areas of application and adoption of QCR sensors from online measurement of industrial processes and high-throughput biomolecular interaction analysis to domestic gadgets.

7. Conclusion

In this paper, we presented a new method for measurement of resonance frequency and dissipation of resonators, with a particular attention to quartz crystal resonators (QCRs). The method is based on an analytical formula that is derived using the equivalent electrical circuit of a resonator. The analytical formula allows direct and continuous measurement of the resonance frequency and dissipation from each impedance datapoint using a fixed frequency drive without the need for any numerical fitting or measurement dead time. This enabled nearly two orders of magnitude better time resolution of measurement with superior noise performance compared to the fastest QCR reported in the literature. This was demonstrated both theoretically and experimentally using quick needle touches on a biotin thiol functionalised QCR in liquid. Measurements of resonance frequency and dissipation for mass and viscous loading experiments showed encouraging quantitative agreement with impedance analysis method over the resonance bandwidth. Improvements in the accuracy of the calibration and the electrical equivalent circuit model could further improve the quantitative agreement. The simplicity of the method could potentially expand the use of quartz crystal resonators in industrial, clinical and domestic applications at lower costs per unit through enabling greater multiplexability and scalable single-chip integration.

8. Materials and methods

8.1. Instrument

A nonlinear network analyser was designed and built in-house and used for our experiments. The instrument is unique with the capability of driving with a wide range of amplitude (0–40 V) and frequency (RF 100 kHz to 300 MHz) and recording complex (in-phase and quadrature) current and voltage sensitively (noise $\sim 1\mu V/\sqrt{Hz}$) and synchronously at 3 frequencies of choice. For the experiments in this paper, only one receiving frequency was used, which was equal to the drive frequency. The instrument is capable of being driven at linearly varying frequency at fixed amplitude (used for impedance analysis method), at linearly varying amplitude at fixed frequency and at fixed amplitude and frequency (used for FFD method).

A graphical user interface was developed and installed on a PC to communicate with the instrument. Wolfram Mathematica10 was used to analyse the data.

A syringe pump (Harvard Apparatus) was used for controlled and measured delivery of sample into the sensor.

A commercial bench-top Vector Network Analyzer (VNWA 3E, SDR-Kits, UK) was used in the experiment for continuous monitoring of biotin-streptavidin binding to compare the results with FFD method.

8.2. Reagents

Acetone, isopropanol, ultra-pure 200-proof ethanol, phosphate buffered saline (PBS) and streptavidin were obtained from Sigma-Aldrich (UK). PBS consisted of 8.1 mM Na_2HPO_4, 1.1 mM KH_2PO_4, 1 mM $MgCl_2$, 2.7 mM KCl, and 138 mM NaCl with a pH of 7.4. Deionised (DI) water was obtained from a Milli-Q Integral system, Millipore, USA. Thiolated alkane solutions, namely HS-(CH_2)11-EG6-Biotin and HS-(CH_2)11-EG3-OCH_3, were obtained from ProChimia (Poland).

8.3. Quartz crystal resonator

14.3 MHz AT-cut thickness-shear mode quartz crystal resonators (dia: 8.3 mm, thickness: 115 μm) were procured from LapTech Precision Inc., Bowmanville, Ontario, Canada. The quartz substrate was sandwiched between two circular gold electrodes on the top and bottom of diameters 5 mm and 4 mm respectively. The top electrode was wrapped around to ensure electrical connection from the bottom side.

8.4. Sensor assembly

The sensor assembly comprised three main parts: microfluidic cartridge, quartz crystal resonator (QCR) and printed circuit board (PCB) (Fig. 1d). An exploded cross-sectional view of all the sub-parts is shown in Fig. 1d-ii.

8.4.1. Microfluidic cartridge

The microfluidic cartridge consisted of two injection molded cyclic olefin copolymer (COC) slides (Microfluidic ChipShop GmbH, Germany) that were bonded together by a medical-grade ARcare® 90106 double-sided pressure-sensitive adhesive (Adhesive Research Inc., Ireland). The top COC slide had integrated mini-luer connectors for fluidic interfacing into which silicone gaskets made of tube stubs were fitted, allowing for a liquid-tight seal with external tubing. The bottom COC slide was milled to include two vertical fluidic interconnects serving as inlet/outlet to the sample chamber above the QCR, and a circular trench centered on the bottom side into which a UPS VI classified EPDM O-ring (Trelleborg AB, Sweden) was inserted. Microfluidic channels were patterned in the adhesive film by CNC cutting, connecting the mini-luer connectors on the top COC slide with the two vertical interconnects on the bottom COC slide.

8.4.2. PCB

The printed circuit board was based on a standard FR4/Cu PCB laminate to which a 1 μm Au layer with a 0.1 μm TiW adhesion layer was sputtered to provide a non-oxidizing metal surface suitable for repeatable electrical contact. Isolated electrical lines and neighboring grounded areas were patterned on the PCB by CNC milling to provide contact pads for the quartz crystal resonator and conductive lines to two SMA coaxial connectors soldered onto each end of the board. Four holes were drilled in the PCB, into which straight brass pins were inserted, serving as alignment structures during assembly of the cartridge. A polycarbonate spacer was aligned to the brass pins and added to the patterned surface of the PCB. The spacer was patterned using CNC milling to form a centered hole that fitted and aligned with the quartz crystal during final assembly.

The abovementioned three parts were assembled by first placing the QCR in the centered hole of the spacer on the PCB so that the electrodes on the bottom side of the quartz crystal made contact with the electrical contact pads patterned on the PCB. Thereafter, the microfluidic cartridge was clamped on top of the QCR and the PCB, forming a sample chamber with a volume of 3 μL above the QCR. The spacer provided a

physical stop when the parts were clamped together, thus limiting the maximum pressure applied to the QCR. The quality factor of the assembled QCR was measured as ~2000 in liquid, suggesting minimal damping by the O-ring.

8.5. Protocol for cleaning of QCR

The QCR was placed in a Petri dish and cleaned using ultrasonication, first in acetone (5 min) and then in isopropanol (10 min). The crystal was then dried in nitrogen flow and further cleaned in argon plasma for 45 s using a Harrick Plasma Cleaner.

8.6. Protocol for formation of self-assembled monolayer of thiol on QCR

Cleaned QCRs were placed in 24-well plate and immersed in 250 µL of 1 mM ethanolic solution of a mixture of thiols containing 10% biotin thiol (HS-(CH_2)11-EG6-Biotin) and 90% methoxy thiol (HS-(CH_2)11-EG3-OCH_3) by volume for about 18 h for the formation of a self-assembled monolayer of thiols.

Acknowledgements

The authors acknowledge the contributions of Dr Alexander Zhukov of University of Cambridge for development of the graphical user interface of the nonlinear network analyser instrument, the EU projects RAPP-ID (FP7-JTI 115153) and Norosensor (FP7-NMP 604244), and the EPSRC Bridging the Gap in Antimicrobial Resistance grant (EP/M027341/1) for covering the cost of instrument development and consumables, and Wolfson School for supporting the PhD studentship of Arnab Guha.

Appendix A. Supplementary data

Supplementary material related to this article can be found, in the online version, at doi:https://doi.org/10.1016/j.snb.2018.11.052.

References

[1] A.-S. Rollier, M. Faucher, B. Legrand, D. Collard, L. Buchaillot, Electrostatic Actuators Operating in Liquid Environment: Suppression of Pull-in Instability and Dynamic Response, arXiv Prepr. arXiv0711.3321 (2007).
[2] P.L.T.M. Frederix, M.R. Gullo, T. Akiyama, A. Tonin, N.F. De Rooij, U. Staufer, A. Engel, Assessment of insulated conductive cantilevers for biology and electrochemistry, Nanotechnology 16 (2005) 997–1005, https://doi.org/10.1088/0957-4484/16/8/001.
[3] D.A. Buttry, Applications of the quartz crystal microbalance to electrochemistry, Electroanal. Chem. – A Ser. Adv. 17 (1991) 1–86.
[4] M.R. Deakin, D.A. Buttry, Electrochemical applications of the quartz crystal microbalance, Anal. Chem. 61 (1989) 1147A–1154A, https://doi.org/10.1021/ac00195a001.
[5] N. Balke, S. Jesse, B. Carmichael, S.V. Kalinin, A.N. Morozovska, L. Qing, S. Jesse, S.V. Kalinin, S. Jesse, A.P. Baddorf, S.V. Kalinin, R. Wagner, J.P. Killgore, R.C. Tung, N. Balke, S. Jesse, P. Yu, B. Carmichael, Quantification of surface displacements and electromechanical phenomena via dynamic atomic force microscopy, Nanotechnology 27 (2016) 1–12.
[6] C. Koblinger, E. Uttenthaler, S. Drost, F. Aberl, H. Wolf, G. Brink, A. Stanglmaier, E. Sackmann, Comparison of the QCM and the SPR method for surface studies and immunological applications, Sens. Actuators B Chem. 24 (1995) 107–112, https://doi.org/10.1016/0925-4005(95)85023-6.
[7] A.J. Slavin, Stabilization of sample temperature in a surface-science vacuum chamber to 0.03 K and quartz-crystal microbalance frequency to 0.06 Hz over 0.5 h, Rev. Sci. Instrum. 81 (2010) 0–5, https://doi.org/10.1063/1.3488368.
[8] B.N. Johnson, R. Mutharasan, Biosensing using dynamic-mode cantilever sensors: a review, Biosens. Bioelectron. 32 (2012) 1–18, https://doi.org/10.1016/j.bios.2011.10.054.
[9] P. Prakrankamanant, Quartz crystal microbalance biosensors: prospects for point-of-care diagnostics, J. Med. Assoc. Thai. 97 (2014).
[10] C. Ricciardi, G. Canavese, R. Castagna, I. Ferrante, A. Ricci, S.L. Marasso, L. Napione, F. Bussolino, Integration of microfluidic and cantilever technology for biosensing application in liquid environment, Biosens. Bioelectron. 26 (2010) 1565–1570, https://doi.org/10.1016/j.bios.2010.07.114.
[11] R.L. Bunde, E.J. Jarvi, J.J. Rosentreter, Piezoelectric quartz crystal biosensors, Talanta 46 (1998) 1223–1236, https://doi.org/10.1016/S0039-9140(97)00392-5.
[12] M. Ferrari, V. Ferrari, An oscillator circuit for dual-harmonic tracking of frequency and resistance in quartz resonator sensors, Meas. Sci. Technol. 20 (2009), https://doi.org/10.1088/0957-0233/20/12/124005.
[13] R. Borngräber, J. Schröder, R. Lucklum, P. Hauptmann, Is an oscillator-based measurement adequate in a liquid environment? IEEE Trans. Ultrason. Ferroelectr. Freq. Control 49 (2002) 1254–1259, https://doi.org/10.1109/TUFFC.2002.1041542.
[14] C. Chagnard, P. Gilbert, A.N. Watkins, T. Beeler, D.W. Paul, An electronic oscillator with automatic gain control: EQCM applications, Sens. Actuators B Chem. 32 (1996) 129–136, https://doi.org/10.1016/0925-4005(96)80121-3.
[15] D. Johannsmann, The Quartz Crystal Microbalance in Soft Matter Research: Fundamentals and Modeling, (2014), https://doi.org/10.1007/978-3-319-07836-6.
[16] E.A. Vittoz, M.G.R. Degrauwe, S. Bitz, High-performance crystal oscillator circuits: theory and application, IEEE J. Solid-State Circuits 23 (1987) 774–783, https://doi.org/10.1109/4.318.
[17] I.D. Avramov, A 0-phase circuit for QCM-based measurements in highly viscous liquid environments, IEEE Sens. J. 5 (2005) 425–432, https://doi.org/10.1109/JSEN.2004.841450.
[18] A. Arnau, Y. Montagut, J.V. García, Y. Jiménez, A different point of view on the sensitivity of quartz crystal microbalance sensors, Meas. Sci. Technol. 20 (2009) 124004, , https://doi.org/10.1088/0957-0233/20/12/124004.
[19] S. Jayasvasti, D. Isarakorn, S. Nundrakwang, Comparative study of QCM analyzers based on pierce oscillator and electromechanical impedance techniques, BMEiCON 2016 - 9th Biomed. Eng. Int. Conf. (2017), https://doi.org/10.1109/BMEiCON.2016.7859608.
[20] F. Eichelbaum, R. Borngräber, J. Schröder, R. Lucklum, P. Hauptmann, J. Schro, R. Borngra, Interface circuits for quartz-crystal-microbalance sensors, Rev. Sci. Instrum. 70 (1999) 2537–2545, https://doi.org/10.1063/1.1149788.
[21] F. Wudy, M. Multerer, C. Stock, G. Schmeer, H.J. Gores, Rapid impedance scanning QCM for electrochemical applications based on miniaturized hardware and high-performance curve fitting, Electrochim. Acta 53 (2008) 6568–6574, https://doi.org/10.1016/j.electacta.2008.04.079.
[22] Z. Farka, D. Kovář, P. Skládal, Rapid detection of microorganisms based on active and passive modes of QCM, Sensors (Switzerland) 15 (2015) 79–92, https://doi.org/10.3390/s150100079.
[23] G. Liu, Z. Dong, D. Li, Y. Wang, Impedance Measurement of Quartz Crystal Based on Network Analysis Method, (2010), p. 79972N, https://doi.org/10.1117/12.888541.
[24] M. Rodahl, B. Kasemo, Frequency and dissipation-factor responses to localized liquid deposits on a QCM electrode, Sens. Actuators B Chem. 37 (1996) 111–116, https://doi.org/10.1016/S0925-4005(97)80077-9.
[25] M. Edvardsson, M. Rodahl, B. Kasemo, F. Höök, A dual-frequency QCM-D setup operating at elevated oscillation amplitudes, Anal. Chem. 77 (2005) 4918–4926, https://doi.org/10.1021/ac050116j.
[26] G. Ohlsson, C. Langhammer, I. Zorić, B. Kasemo, A nanocell for quartz crystal microbalance and quartz crystal microbalance with dissipation-monitoring sensing, Rev. Sci. Instrum. 80 (2009), https://doi.org/10.1063/1.3202207.
[27] F. Höök, M. Rodahl, C. Keller, K. Glasmastar, C. Fredriksson, P. Dahiqvist, B. Kasemo, The dissipative QCM-D technique: interfacial phenomena and sensor applications for proteins, biomembranes, living cells and polymers, Time 2 (1999) 966–972, https://doi.org/10.1109/FREQ.1999.841467.
[28] K. Kanazawa, N.J. Cho, Quartz crystal microbalance as a sensor to characterize macromolecular assembly dynamics, J. Sens. 2009 (2009), https://doi.org/10.1155/2009/824947.
[29] A. Pomorska, D. Shchukin, R. Hammond, M.A. Cooper, G. Grundmeier, D. Johannsmann, Positive frequency shifts observed upon adsorbing micron-sized solid objects to a quartz crystal microbalance from the liquid phase, Anal. Chem. 82 (2010) 2237–2242, https://doi.org/10.1021/ac902012e.
[30] J. Petri, S. Hochstädt, T. Nentwig, A. Pausch, A. Langhoff, D. Johannsmann, A fast electrochemical quartz crystal microbalance,which acquires frequency and bandwidth on multiple overtones, Electroanalysis (2016) 1–9, https://doi.org/10.1002/elan.201600580.
[31] Crystal Resonator Chemistry Measurement System (n.d.). https://www.sii.co.jp/jp/segg/files/2013/04/file_PRODUCT_MASTER_1692_GRAPHIC04.pdf (Accessed 23 November, 2017).
[32] Q-Sense E1 Tracking changes at the surface (n.d.). http://www.biolinscientific.com/zafepress.php?url=%2Fpdf%2FQ-Sense%2FProducts%2FE1%2FQS_P_E1brochure.pdf (Accessed 31 July, 2017).
[33] M.E. Yakovleva, G.R. Safina, B. Danielsson, A study of glycoprotein-lectin interactions using quartz crystal microbalance, Anal. Chim. Acta 668 (2010) 80–85, https://doi.org/10.1016/j.aca.2009.12.004.
[34] M.A. Syahbana, D.J.H.D. Santjojo, S.P. Sakti, High-resolution multiple channel frequency counter using spartan-3E FPGA, Proceeding - 2016 Int. Semin. Sensors, Instrumentation, Meas. Metrol. ISSIMM 2016 (2017) 111–114, https://doi.org/10.1109/ISSIMM.2016.7803734.
[35] L. Rodriguez-Pardo, J. Cao-Paz, A. Fariña, A. Covelo, X.R. Nóvoa, C. Pérez, Quartz crystal oscillator sensor for qcm monitoring of water absorption in anticorrosion cataphoretic paintings, 2009 IEEE Int. Freq. Control Symp. Jt. with 22nd Eur. Freq. Time Forum (2009) 1038–1042, https://doi.org/10.1109/FREQ.2009.5168352.
[36] P. Horowitz, W. Hill, The Art Of Electronics, Press Syndicate of the University of Cambridge, Cambridge, 2015.
[37] K.D. Rendulic, A. Winkler, Adsorption and desorption dynamics as seen through molecular beam techniques, Surf. Sci. 299–300 (1994) 261–276, https://doi.org/10.1016/0039-6028(94)90659-9.
[38] A. Rojnuckarin, S. Kim, S. Subramaniam, Brownian dynamics simulations of protein folding: access to milliseconds time scale and beyond, Proc. Natl. Acad. Sci. U. S. A. 95 (1998) 4288–4292, https://doi.org/10.1073/pnas.95.8.4288.

[39] S.K. Ghosh, V.P. Ostanin, A.A. Seshia, Anharmonic interaction signal for acoustic detection of analyte, Anal. Chem. 82 (2010) 0–9, https://doi.org/10.1021/ac100582q.
[40] S. Jose, R. Hueting, A. Jansman, Modelling of bulk acoustic wave resonators for microwave filters, 11th Annu. Work. Semicond. Adv. Futur. Electron. Sensors, SAFE 2008 vol. 1, (2008) 558–561 https://pdfs.semanticscholar.org/5fd5/7702801346ffb87e85fa83ef146890c30b79.pdf%0Ahttp://doc.utwente.nl/65215/.
[41] G. Sauerbrey, Verwendung von Schwingquarzen zur Wägung dünner Schichten und zur Mikrowägung, Zeitschrift Für Phys. 155 (1959) 206–222, https://doi.org/10.1007/BF01337937.
[42] J.R. Vig, E.S. Ferre-Pikal, (IEEE Standard 1139-1999) IEEE Standard Definitions of Physical Quantities for Fundamental Frequency and Time Metrology – Random Instabilities, (1999), https://doi.org/10.1109/IEEESTD.1999.90575.
[43] S. Saha, M. Raje, C.R. Suri, Sandwich microgravimetric immunoassay: sensitive and specific detection of low molecular weight analytes using piezoelectric quartz crystal, Biotechnol. Lett. 24 (2002) 711–716, https://doi.org/10.1023/A:1015238201367.
[44] A. Jbari, L. Bellarbi, N. Zine, C.A. Mills, J. Samitier, A. Errachid, Multiplexed frequency spectrum analyzer instrumentation for the characterization of multiple QCM-based biosensors, 2007 Int. Conf. Sens. Technol. Appl. SENSORCOMM 2007, Proc. (2007) 436–440, https://doi.org/10.1109/SENSORCOMM.2007.4394960.
[45] H. Ogi, H. Nagai, Y. Fukunishi, T. Yanagida, M. Hirao, M. Nishiyama, Multichannel wireless-electrodeless quartz-crystal microbalance immunosensor, Anal. Chem. 82 (2010) 3957–3962, https://doi.org/10.1021/ac100527r.
[46] W. Tao, P. Lin, Y. Ai, H. Wang, S. Ke, X. Zeng, Multichannel quartz crystal microbalance array: fabrication, evaluation, application in biomarker detection, Anal. Biochem. 494 (2016) 85–92, https://doi.org/10.1016/j.ab.2015.11.001.
[47] X. Jin, Y. Huang, A. Mason, X. Zeng, Multichannel monolithic quartz crystal microbalance gas sensor array, Anal. Chem. 81 (2009) 595–603, https://doi.org/10.1021/ac8018697.
[48] Y.-Y. Chen, L.-C. Huang, T.-T. Wu, J.-H. Sun, Isolation of bulk acoustic waves in a sensor array with phononic crystals, 2011 IEEE Int. Ultrason. Symp. (2011) 2487–2490, https://doi.org/10.1109/ULTSYM.2011.0618.
[49] H.H. Lu, Y.K. Rao, T.Z. Wu, Y.M. Tzeng, Direct characterization and quantification of volatile organic compounds by piezoelectric module chips sensor, Sens. Actuators B Chem. 137 (2009) 741–746, https://doi.org/10.1016/j.snb.2009.01.060.
[50] D. Croux, A. Weustenraed, P. Pobedinskas, F. Horemans, H. Diliën, K. Haenen, T. Cleij, P. Wagner, R. Thoelen, W. De Ceuninck, Development of multichannel quartz crystal microbalances for MIP-based biosensing, Phys. Status Solidi Appl. Mater. Sci. 209 (2012) 892–899, https://doi.org/10.1002/pssa.201100715.
[51] C. Garcia-Hernandez, C. Medina-Plaza, C. Garcia-Cabezon, F. Martin-Pedrosa, I. Del Valle, J.A. de Saja, M.L. Rodríguez-Méndez, An electrochemical quartz crystal microbalance multisensor system based on phthalocyanine nanostructured films: discrimination of musts, Sensors (Switzerland) 15 (2015) 29233–29249, https://doi.org/10.3390/s151129233.
[52] G.S. Huang, M. Te Wang, M.Y. Hong, A versatile QCM matrix system for online and high-throughput bio-sensing, Analyst 131 (2006) 382–387, https://doi.org/10.1039/b515722f.
[53] C.A. Mills, K.T.C. Chai, M.J. Milgrew, A. Glidle, J.M. Cooper, D.R.S. Cumming, A multiplexed impedance analyzer for characterizing polymer-coated QCM sensor arrays, IEEE Sens. J. 6 (2006) 996–1001, https://doi.org/10.1109/JSEN.2006.877936.
[54] H. Shen, T. Zhou, J. Hu, A high-throughput QCM chip configuration for the study of living cells and cell-drug interactions, Anal. Bioanal. Chem. 409 (2017) 6463–6473, https://doi.org/10.1007/s00216-017-0591-4.
[55] K. Jaruwongrungsee, U. Waiwijit, A. Wisitsoraat, M. Sangworasil, C. Pintavirooj, A. Tuantranont, Real-time multianalyte biosensors based on interference-free multichannel monolithic quartz crystal microbalance, Biosens. Bioelectron. 67 (2015) 576–581, https://doi.org/10.1016/j.bios.2014.09.047.
[56] A. Tuantranont, A. Wisitsora-at, P. Sritongkham, K. Jaruwongrungsee, A review of monolithic multichannel quartz crystal microbalance: a review, Anal. Chim. Acta 687 (2011) 114–128, https://doi.org/10.1016/j.aca.2010.12.022.